Anal. Chem. **2009,** *81,* 7133–7140

analytical chemistry
feature

Nanofluidics in Lab-on-a-Chip Devices

Michelle L. Kovarik and Stephen C. Jacobson

Indiana University

As the field of nanofluidics matures, fundamental discoveries are being applied to lab-on-a-chip analyses. The unique behavior of matter at the nanoscale is adding new functionality to devices that integrate nanopores or nanochannels. (To listen to a podcast about this feature, please go to the *Analytical Chemistry* website at pubs.acs.org/journal/ancham.)

Advances in microfabrication and miniaturized analysis have resulted in increasingly sophisticated microfluidic systems that are fulfilling the promise of true "labs-on-a-chip" or "micro total analysis systems" by integrating multiple processing steps on a single device.[1] Furthermore, improved fabrication techniques have placed the nanoscale regime within reach, even for laboratories with limited fabrication facilities.[2] These advances are allowing scientists to explore fluidic systems containing conduits that approach molecular-length scales.

Incorporation of biological and synthetic nanochannels in fluidic devices holds great promise for new analytical applications because there are forces and phenomena at this scale that are absent or negligible in larger microchannels.[3] Critical considerations in designing these devices include double-layer overlap (DLO) and the resulting ion permselectivity; localized enhancement of electric fields; and the increased influence of diffusion, surface-to-volume ratio, surface charge, and entropy. Through these effects, nanoscale components can improve routine processing and add new functionality to microfluidic devices.

The goals of this article are to highlight progress in integrated micro- and nanofluidic devices, to demonstrate how nanofluidic components may benefit each function performed during chemical analysis (sample preparation, fluid handling and injection, separation, and detection), and to encourage creative thinking about future applications as this technology matures. This article focuses on devices containing one or more nanochannels or nanopores—fluidic features with at least one dimension typically ≤100 nm. We will discuss discrete features ≤0.5 μm, as opposed to nanoporous monoliths[4] or membranes with tortuous paths,[5] which are reviewed elsewhere.

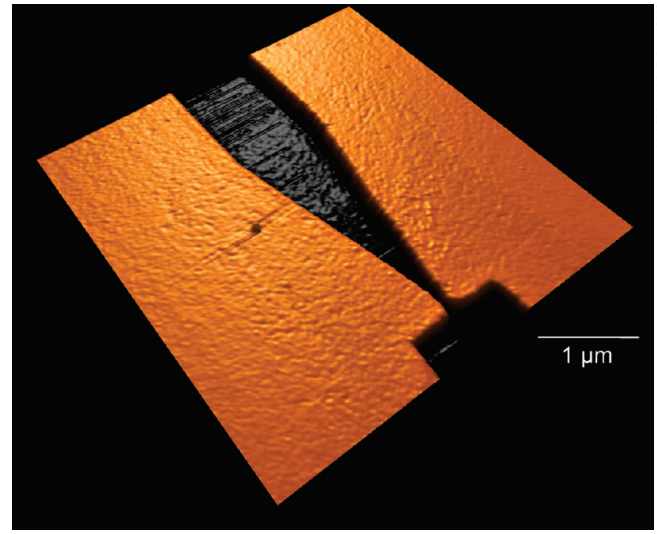

J. M. PERRY AND Z. D. HARMS

Some of the earliest work in nanofluidics used native and engineered protein pores in lipid bilayers to characterize a range of molecules, including polymers, nucleic acids, metal ions, and organic molecules, by resistive-pulse sensing.[10] Protein pores provide excellent reproducibility with respect to their dimensions and internal chemistry and readily self-insert into a bilayer from solution. However, lipid bilayers on-chip are relatively fragile compared to the glass, polymer, and semiconductor substrates typical for microfluidic applications. As a result, many groups are pursuing emerging nanofabrication methods to produce nanochannels in hard and soft materials. Figure 1 shows integrated micro- and nanofluidic devices in which nanopores or channels are formed by a variety of methods, including track-etching polymer membranes,[6] sacrificial layer deposition,[7] electron-beam lithography,[8] and etching photolithographically-defined microchannels to nanometer-scale depths.[9] The variety of available fabrication methods results in flexible device design in which the chemistry and geometry of the nanoconduit are controllable and nanofluidic elements are incorporated either in-plane or out-of-plane.

10.1021/ac900614k CCC: $40.75
Published on Web 08/10/2009

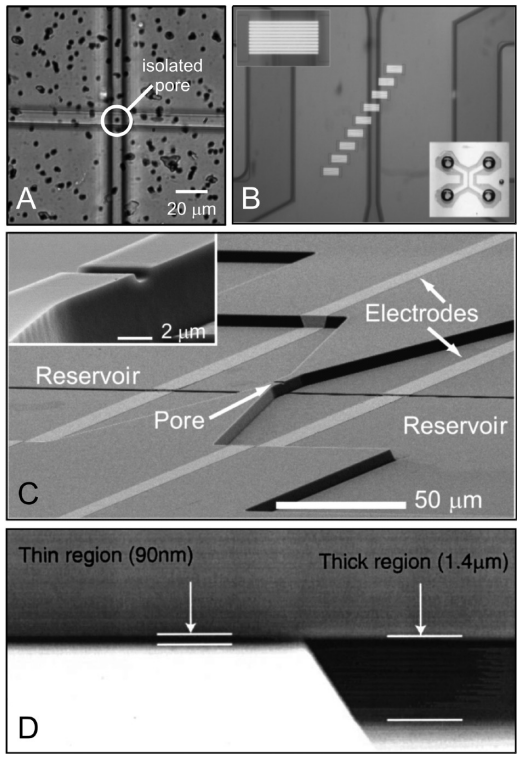

Figure 1. Integrated micro- and nanofluidic devices. (A) A track-etch membrane is sandwiched between two PDMS channels. By tuning the nanopore density and channel width, single conical pores (dark spots), small ensembles, or large numbers of pores connect device layers. Adapted from ref. 6. (B) A sacrificial polysilicon layer is selectively removed to leave arrays of nanochannels. Several sets of nanochannels are patterned so that only one set connects the two microchannels (dark lines). Insets are a close-up of the nanochannels and a view of the device. Adapted from ref. 7. (C) Electron beam lithography defines a nanochannel connecting two microfluidic reservoirs. Inset is a close-up of the nanochannel. Adapted with permission from ref. 8. (D) Two-level photolithography and etching make micrometer-wide channels with regions confined to nanoscale depth. Adapted with permission from ref. 9.

SAMPLE PREPARATION

The goal of lab-on-a-chip systems is sample-in/answer-out capability. A critical and often challenging aspect of these systems is effective sample preparation, which can include filtration, cell lysis, protein digestion, preconcentration, labeling, and other processing steps. These steps are often performed off-chip, but on-chip preparation has been achieved by integrating nanoscale elements on microfluidic devices, improving performance and increasing automation.

The simplest sample preparation step is size-based filtration, which removes particulates before sample introduction on-chip. This step can be integrated on microfluidic devices by incorporating track-etch nanopore membranes on the bottoms of reservoirs for on-chip filtration. This technique eliminates channel clogging and reduces undesirable hydrodynamic flow from unbalanced fluid levels in the reservoirs.[11] Sandwiching a track-etch membrane between two microchannels in a multilayer device is another way to achieve on-chip filtration; either the filtrate, which passes through the membrane, or the retentate, which is retained in the microchannel, can be analyzed.[12] Both modes have been evaluated by placing a polycarbonate membrane containing 10-nm pores between two PDMS channels. In one analysis, researchers separated filtrate containing glutathione from matrix interferents, such as proteins in plasma or cell lysate, prior to detection. In a different application, the retentate, containing a PCR product, was concentrated at the membrane surface for analysis while smaller primer DNA strands were washed away.

The high surface-to-volume ratio of nanostructured materials is also useful for sample preconcentration. Insulin has been selectively preconcentrated by microfluidic patterning of immobilized Fab′ on a nanopore membrane, followed by MALDI MS analysis.[13] Although the actual concentration and detection steps were not performed on-chip, microfluidic patterning of nanopore membranes could be scaled up to create arrays of immobilized antibodies for multiplexed sensing. In addition to antibodies, a wide range of chemical functionalities can be grafted onto track-etch membranes and their inner pore surfaces for use in preconcentration, protein digestion, or labeling reactions.

Electrokinetic sample preconcentration is possible at microchannel−nanochannel junctions because of unique ion transport phenomena in these regions.[4] Applying electric fields across these devices causes unbalanced ion flux, or concentration polarization, across the nanochannel, resulting in analyte concentration at the anodic and/or cathodic ends of the nanochannel. Several examples are reported of electrokinetically induced concentration polarization caused by DLO. In these cases, co-ions (typically anions because most device materials have negative surface charge) are excluded from the nanochannel. Cations are selectively transported through the nanochannel, resulting in unbalanced cation flux.[14] Electrostatic exclusion traps anions on the cathodic side of the nanochannel, where they concentrate with cations to maintain local electroneutrality. At the anodic side, cations depart through the nanochannel toward the cathode, anions travel to the anode without being replaced, and an ion depletion region forms. This depletion leads to sample concentration at the anodic end of the nanochannel because analyte ions stack at the boundary of the depletion region (Figure 2A).[15] This preconcentration improved the dynamic range and sensitivity of a bead-based immunoassay.[16]

Concentration polarization also occurs in the absence of DLO.[6] In this case, ion depletion develops because a large proportion of current through the nanopore is carried by counterions, resulting in depletion on the anodic side. This illustrates that electrokinetic preconcentration can be performed on devices using larger pores or higher ionic strengths than would be possible if DLO were required. Figure 2B−D shows examples of electrokinetic preconcentration due to concentration polarization.

Electrophoretic and dielectrophoretic concentration of particles and cells is possible using conical nanopores in microfluidic devices.[17] Because nanoscale components are usually the most resistive elements on integrated devices, electric potentials across nanopores yield high electric field strengths and gradients from modest applied voltages. The resulting electrophoretic and dielectrophoretic forces trap particles at the small diameter opening of conical nanopores. These devices could be used for selective preconcentration of specific cell types based on their different dielectrophoretic responses. Cell lysis may also be possible using the high local electric fields associated with nanoscale conduits.

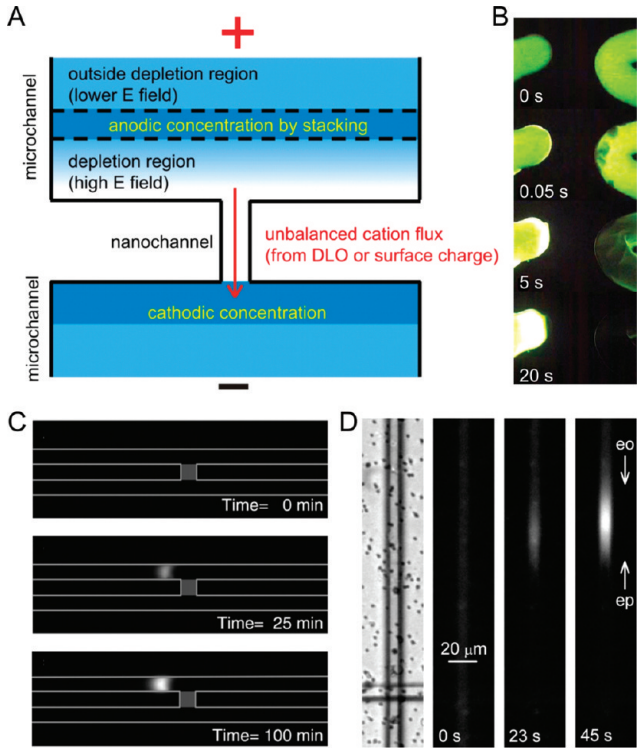

Figure 2. Electrokinetic sample preconcentration. (A) Concentration polarization at a microchannel−nanochannel junction due to DLO or surface-charge effects. (B) Fluorescein concentrates on the cathodic side (left) and is depleted at the anodic side (right) of nanochannels (not visible). Adapted from ref. 14. (C) GFP concentrates by stacking near the depletion region on the anodic side of nanochannels (gray). Adapted from ref. 15. (D) Surface charge induced ion depletion causes stacking of fluorescein in the microchannel at the anodic side of a multilayer nanopore device. Adapted from ref. 6.

FLUID HANDLING: SAMPLE INJECTION, TRANSPORT, AND MIXING

Improved performance of microfluidic systems (versus traditional capillary separations) is often attributed to improved sample injection: channel interconnects with minimal dead volumes decrease dispersion. Miniaturized devices have been applied to a number of problems that require precise fluid handling. Nanofluidic components will push this trend to even smaller volumes. Though unique transport phenomena and diffusion in nanochannels present challenges to fluid handling, volumes as small as ~50 aL have been electrokinetically dispensed (Figure 3A),[18] and simple pressure gating can pump, filter, and trap analytes in elastomeric nanochannels.[19]

While single nanochannels can manipulate and inject ultrasmall sample volumes, nanofluidic arrays, which have voltage-switchable gating, present an attractive injection scheme for microfluidic separations.[20] Injections are implemented on multilayer devices by sandwiching a nanopore membrane between two device layers (as in Figure 1A, but with many pores at the intersection), adding functionality without a significant increase in footprint. Separating device layers with nanopore membranes prevents uncontrolled mixing and facilitates voltage-gated injections between layers. Unbiased sample injection is performed using large pores (200-nm diameter), whereas molecular-weight-based filtration is combined with injection using smaller pores (15-nm diameter). Additionally, postseparation valving with nanopore membranes can extract peaks of interest from the separation channel into another device layer for further analysis (Figure 3B).[20]

Electrokinetic gating is also possible with nanofluidic transistors. These devices contain gate electrodes separated from the nanochannel by a thin dielectric layer. Electric fields from these electrodes penetrate the entire depth of a nanochannel, allowing them to control ion transport in the device. For example, in a device with negative surface charge, applying a negative voltage enriches cations, which are the primary charge carriers, and increases conductance. A positive gate potential has the opposite effect. Concentration and transport of dyes,[22] DNA,[23] and avidin[24] have been controlled in this fashion. In a recent report of a pH- and ionic-strength-controlled transistor, researchers produced the effect of a gate electrode in an hourglass-shaped nanopore by controlling its surface charge (Figure 3C).[21] This system could be incorporated in a multilayer device for chemically-controlled electrostatic gating.

Nanochannels can also be gated by steric methods. In these cases, the channel surface is modified with a macromolecular coating that controls transport through the nanoconduit. Some systems, such as conical nanopores modified with DNA, offer voltage-controllable ion permselectivity.[25] When a positive potential was applied to the small diameter side of a modified pore, the DNA strands were drawn out of the pore, resulting in an "on" state. When the potential was reversed, DNA was drawn into the tip, blocking the pore and creating the "off" state. Chemical switches can also control steric gating. Nanoporous alumina membranes modified with adsorbed surfactants gated the transport of small molecules such as methyl viologen and fluorescein,[26] and simulations have suggested that polymer brushes could perform steric gating using solvent composition to control the coil-to-globule transition of the polymer.[27] None of these steric-based systems has been integrated on-chip yet, and chemically-gated examples have limited temporal resolution compared to electrokinetic switching. However, for applications that require chemical rather than electrokinetic switches, they provide alternative valving mechanisms.

Nanofluidic components also provide electrically-controlled, pressure-driven fluid flow for applications requiring fluid transport through field-free regions (for example, efficient transport of cells without electroporation or lysis). When electroosmotic flow is directed from a microchannel through a nanoconduit, not all of the electroosmotically pumped fluid from the microchannel passes through the nanochannel to the cathode because of the electroosmotic flow properties of the nanochannel. The result is superambient or subambient pressure at the microchannel−nanochannel junction that induces bulk fluid flow in the field-free region of the microchannel downstream of the nanoconduit—a phenomenon called electroosmotically induced hydraulic pumping.[28] This mechanism could be useful for portable devices because it generates pressure-driven flow without an external pump.

Some applications require controlled mixing or prevention of mixing of one or more liquid streams. Laminar flow in microchannels minimizes mixing, and nanopore membranes or nanochannel arrays further reduce convective flow between the connected microchannels because of the fourth-power dependence of pressure-driven flow on the lateral dimensions of a channel. Thus,

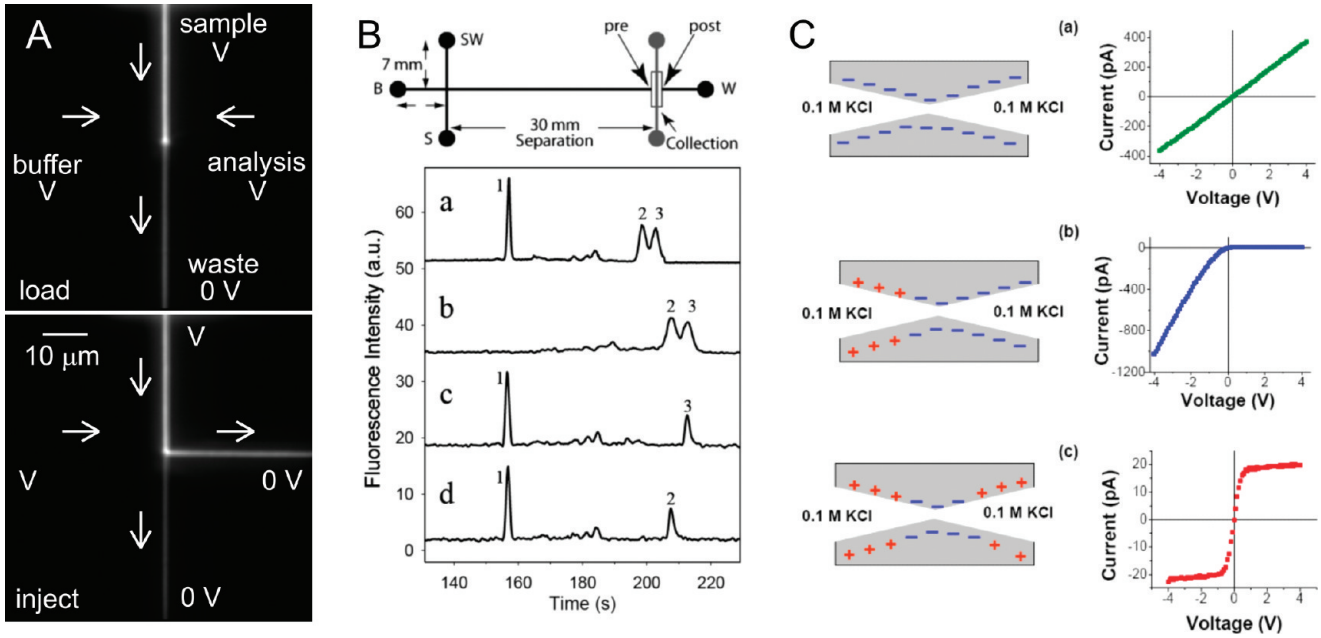

Figure 3. Fluid control on nanofluidic devices. (A) Fluorescence images of a modified pinched injection developed to control sample diffusion through nanochannel intersections. This device dispenses volumes ≥50 aL. Adapted from ref. 18. (B) A nanopore membrane connecting two device layers controls valving between channels. Trace (a) shows an electropherogram for separation of glutamate (peak 1) and arginine (peaks 2 and 3) labeled with FITC. Traces (b−d) show selective extraction of each peak through a nanopore membrane into another device layer. Adapted from ref. 20. (C) An hourglass-shaped nanopore in which the current−voltage behavior is controlled by adjusting the surface charge inside the pore. Adapted with permission from ref. 21.

different solution compositions are maintained on opposite sides of a nanofluidic connection with only diffusive mixing, even with a substantial pressure difference between the two sides. Researchers harnessed this effect for diffusive sensing of calcium ions, bacterial cells, and enzyme activity.[29] For these applications, eliminating convective flow at each array intersection ensured that only solutions directly across the membrane from each other reacted without substantial mass transfer across the membrane. Combining this effect with DLO resulted in stable pH gradients between two device layers.[30]

In contrast to the above examples, some applications, especially on-chip reactions, require fast and efficient mixing of solutions on-chip. A well-defined 3D nanochannel network fabricated within a microchannel provided efficient passive mixing.[31] This mixer performed well at higher fluid velocities and over shorter distances than previously reported random nanoporous mixers. Gated injections through nanopore membranes also enhanced mixing and were used in chip-based lead sensors.[32] Electrically actuated injection was used to mix sample with electrospray buffer prior to MS; as an added benefit, injection through the nanopores partially desalted the sample.[33] This work suggests that after electrophoretic separation in one device layer, an analyte plug could be quantitatively transferred across the membrane for mixing with electrospray buffer, ionization, and MS analysis.

SEPARATION

Integrated micro- and nanofluidic devices are advancing separations by improving the performance of traditional separations and development of separations based on entropy and other effects that dominate at molecular-length scales.[34] One of the earliest promises of microfabrication was uniform, regular stationary phases to simplify fabrication and minimize dispersion from random packing.[35] More recently, examples of nanopillar arrays for biomolecule separations based on Ogston sieving, reptation, and entropic recoil have been reported.[36,37] Employing discrete nanochannels in separation systems offers several advantages as well.

Devices incorporating alternating deep (1.8 μm−300 nm) and shallow (55−73 nm) regions (Figure 1D) elucidate what had been considered gel-based separation mechanisms. In gels and nanofluidic devices, the characteristic length scale of the separation space approaches that of individual molecules, resulting in separation by entropic trapping or Ogston sieving.[38] In entropic trapping, long molecules, such as 5−160 kilobase-pair (kbp) DNA, passing through the channel are entropically trapped at the entrances of shallow regions. Escape from the trap requires that a critical number of base pairs enters the nanoscale constriction so that the rest of the molecule is pulled through to the next deep region (Figure 4A). Longer molecules with larger radii of gyration present more surface area to the entropic trap, increasing the probability that the requisite number of base pairs will enter the shallow region. Higher mobility for larger molecules yields an entropy-based separation.[39]

For smaller analytes, such as short strands of DNA, the radius of gyration can be smaller than the characteristic channel dimension, and Ogston sieving becomes the dominant separation mechanism. In this technique, elution order is from smallest analyte to largest, with analyte mobility proportional to the fraction of the nanoscale constriction accessible to the molecule (Figure 4C). This effect permitted separation of SDS−protein complexes and short (50−766 bp) DNA strands.[40]

Both entropic trapping and Ogston sieving are observed in gel electrophoresis. In discrete nanofluidic devices, however, the separation matrix is precisely fabricated to pinpoint the transition

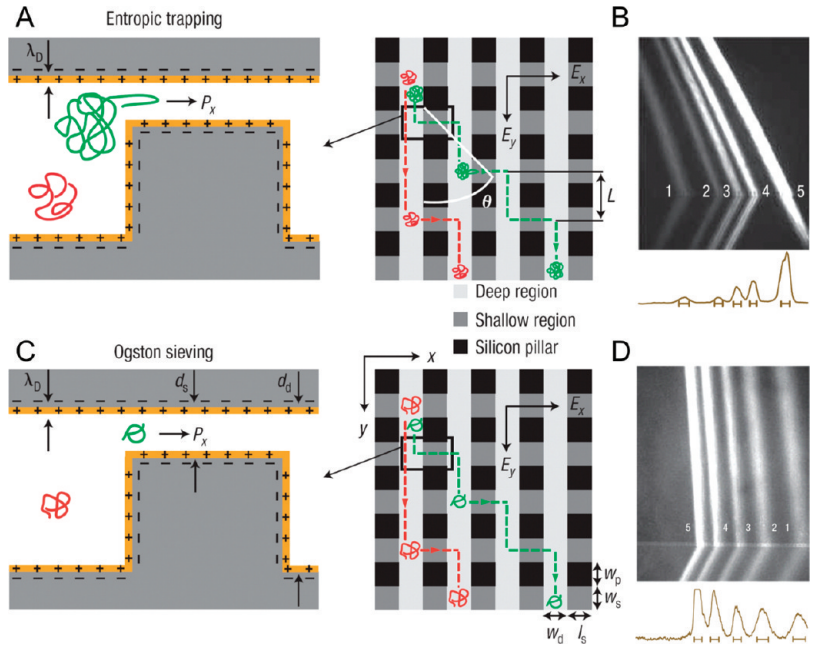

Figure 4. Gel-free DNA separations in a continuous-flow nanofluidic device. (A) Entropic trapping in a nanofilter device. (B) Separation by entropic trapping of λ-DNA−Hind III digest: (1) 2322, (2) 4361, (3) 6557, (4) 9416, and (5) 23,130 bp. Mobility—and therefore deflection angle—increases with DNA length. (C) Ogston sieving in a nanofilter device. (D) Continuous separation of PCR markers: (1) 50, (2) 150, (3) 300, (4) 500, and (5) 766 bp, showing the increase in mobility from largest to smallest analyte, characteristic of Ogston sieving. Adapted with permission from ref. 41.

between these two mechanisms. One example is a planar device for continuous-flow separation that has alternating rows of shallow and deep channels. The shallow nanoscale channels are blocked at regular intervals by solid pillars that support the device structure (Figure 4). The versatility of this device is evident from the variety of separations demonstrated, including entropic trapping separation of λ-DNA−Hind III digest (Figure 4B), Ogston sieving of PCR markers (Figure 4D), and separation of proteins by Ogston sieving at high ionic strength and by electrostatic sieving at low ionic strength.[41]

In this device, sample was introduced in the upper left corner, and electric fields applied in the *x* and *y* directions. Analytes with higher mobilities were more likely to jump across the shallow regions as they traversed the array, underwent greater deflection, and exited the array further to the right. The transition between entropic trapping and Ogston sieving was identified by examining deflection angle as a function of DNA length. Deflection and mobility decreased with increasing strand length up to ~1 kbp, indicating Ogston sieving. For ≥2 kbp, deflection and mobility increased with chain length, corresponding to entropic trapping. These integrated micro- and nanoscale devices perform gel-free separations of a wide range of biomolecules simply by adjusting device dimensions or ionic strength to tune the separation mechanism.

In open-channel chromatographic separations, mass transfer improves significantly with reduced channel dimensions because of the efficiency of diffusion over nanometer-scale distances. The major obstacle to nanoscale LC is the enormous pressure drop required to produce optimum fluid velocities using traditional pressure-driven pumping. Shear-driven flows, however, provide high fluid velocities in nanoscale channels by means of a moving wall, which drags fluid through the nanochannel. Using shear-driven flow, researchers separated peptides in <1 second in 120-nm deep nanochannels modified with C12 and C18 coatings.[42] Samples contained only two to four components but nevertheless demonstrated the potential for nanoscale LC.

Some electrophoretic separations also benefit from reduced channel dimensions because of the effects of DLO. DLO induces in a parabolic (rather than plug-like) electroosmotic flow profile and a subsequent decrease in the radially-averaged electroosmotic velocity.[43] This phenomenon is exploited to perform a version of hydrodynamic chromatography: analytes are separated based on size because they sample the radially-varying electroosmotic flow differently. Using 320-nm deep channels and 0.2-mM background electrolyte, 100-bp and 1000-bp double-stranded DNA were resolved under free-solution conditions. In this separation, the larger DNA strand eluted first because the smaller strand, with its smaller radius of gyration, more closely approached the lower velocity region near the channel walls, reducing its average velocity.[44] The same effect resolved a 10−100-bp DNA ladder in a 100-nm channel at 1-mM buffer concentration.[45] The elution order reversed at higher ionic strengths in the absence of DLO. Interestingly, large-to-small elution was observed for 1560-nm deep channels, which do not exhibit DLO at any electrolyte concentration tested. This elution order was attributed to additional charge from the FITC label, which contributed disproportionately to the charge-to-hydrodynamic-drag ratio of shorter DNA strands. This indicates that in nanoscale separations, the effects of DLO and ionic strength require careful consideration and present additional variables for improving resolution.

DLO and the resulting parabolic flow also allow electrophoretic separations based on valence. In an array of high-aspect ratio nanochannels, anionic Alexa 488 eluted before neutral Rhodamine B because Alexa 488 was repelled from the negatively-charged nanochannel walls and confined to the faster flow in the center of the nanochannels.[46] Rhodamine B sampled all radial velocities

evenly and adsorbed slightly to the nanochannel walls. The elution order reversed when the separation was performed in a microchannel. Carboxyl fluorescein (charge of −2) and bodipy (charge of −1) separated similarly in a single nanochannel.[47] In this case, the elution order was the same for a 40-nm deep channel and a 2-μm deep channel. However, the distance between bands decreased in the nanochannel because the carboxyl fluorescein spent more time in the faster flow in the center of the nanochannel. The valence and mobility of each analyte were calculated by comparing the analyte velocity in each channel.

DETECTION

For detection methods such as absorbance, the decreased path lengths and sample volumes analyzed in micro- and nanofluidics are problematic. Other methods such as electrochemistry and fluorescence scale well with decreasing device dimensions, and in many cases, reduced detection volumes even improve sensitivity. For example, the efficiency of diffusive transport in nanochannels makes them ideal for redox cycling because oxidation products rapidly diffuse across the nanochannel to the opposite electrode for reduction.[48] Another potential advantage in nanofluidic systems is that the detection volume approaches the scale of individual molecules. As a result, integrated micro- and nanofluidic systems are well-suited for applications requiring single-molecule detection. The limited volume of a nanoconduit makes it appropriate for single-molecule fluorescence studies at biologically relevant concentrations and for resistive-pulse sensing.

When fluorescent molecules are confined in nanochannels, the limited detection volume allows individual molecules to be observed from a bulk solution of relatively high concentration (Figure 5A). Individual quantum dot conjugates have been detected in nanochannels with 500-nm × 500-nm cross-sections,[49] and both single-molecule detection and fluorescence correlation spectroscopy of Alexa Fluor 488-5-dUTP have been performed in smaller channels.[50] The S/N in the nanochannel device nearly doubles compared to traditional open-solution measurements because of reduced Raman scattering by solvent molecules and consistent excitation of analyte molecules, which are confined by the channel walls to the center of the illumination—every molecule passing through the detection volume contributes to the analysis. This capability, combined with extremely low volumetric flow rates, makes nanofluidic devices ideal for small-volume samples. Also, improved S/N and the ability to use a pseudo-1D model allow shorter analysis times when performing autocorrelation in the nanochannel device. Single fluorescent molecules have also been detected as they transit a nanopore in an aluminum/silicon nitride membrane; the opacity of the membrane eliminates background fluorescence from sample above the membrane.[51] Opaque nanopore membranes could be incorporated into multilayer microfluidic devices for single-molecule fluorescence detection in an out-of-plane format.

Because single-molecule measurements examine each analyte molecule individually, nanofluidic detection elements can relax the demand for physical separation of sample components prior to detection. Photon bursts from individual stained DNA fragments have been observed in a 1-μm wide, 270-nm deep nanochannel.[52] Because the intensity of the photon burst is proportional to the length of the fragment, histograms of single-molecule data reveal the size distribution of a DNA ladder without the need for separation. Additionally, the frequency of each level of burst intensity provides the relative concentrations of the fragments (Figure 5C). DNA restriction mapping can also be performed without separating the restriction fragments.[53] In one case, single λ-phage DNA molecules were confined in 100−200-nm diameter channels and reactions with three different restriction enzymes recorded in real time. The lengths of the resulting fragments were determined from fluorescence intensity data after the fragments diffused apart. Single-molecule mobility measurements of nucleic acid fluorescent labels in submicrometer channels yielded infor-

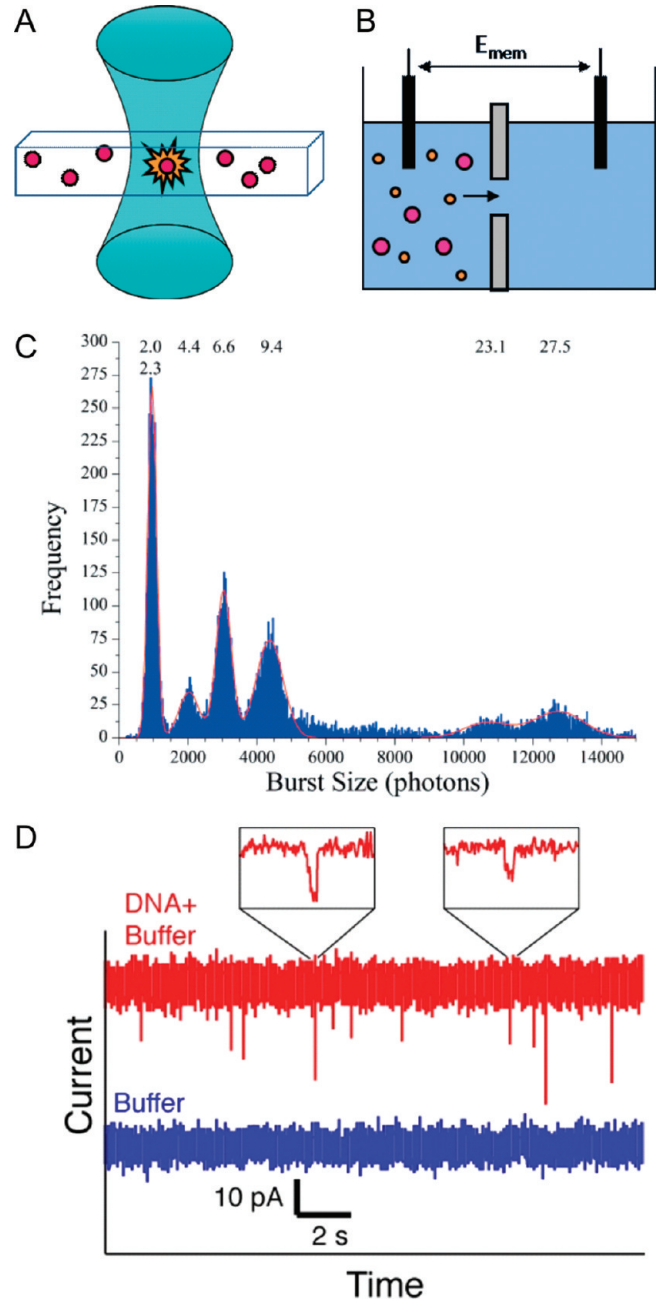

Figure 5. Nanofluidic detection methods. (A) Single-molecule fluorescence in a nanochannel. (B) Resistive-pulse sensing using a nanopore. E_{mem} is the transmembrane potential. (C) Histogram of photon bursts for single-molecule fluorescence measurements of a DNA mixture. All strand sizes except 2.0 and 2.3 kbp are resolved without the need for separation. Adapted from ref. 52. (D) Resistive-pulse measurement of λ-phage DNA using a 200-nm wide, 200-nm deep nanochannel. Adapted from ref. 60.

mation typically obtained by electrophoresis without physical separation of sample components.[54]

Nanopores can also be used for on-chip resistive-pulse sensing, a single-molecule detection method that measures the change in current when a particle enters a pore connecting two conducting solutions (Figure 5B).[10] The most common example is Coulter counting, but all applications rely on one basic principle: if a particle displaces a sufficient fraction of electrolyte, a measurable change in the pore resistance and a corresponding change in current are produced. With a sufficiently small aperture, single porphyrin molecules were detected,[55] and nanopore resistive-pulse sensing has been suggested as a next-generation DNA sequencing technique.[56]

Although fabrication is challenging, lipid bilayers with protein pores can be integrated in microfluidic devices. Three approaches have been demonstrated: using external pressure to thin a lipid solution down to a bilayer,[57] exploiting the material properties of PDMS to extract excess solvent,[58] and painting a lipid solution onto an aperture through an access hole in the device.[59] The interaction of polyethylene glycol chains with an α-hemolysin protein channel has been observed with the latter device.

The technical difficulty of fabricating robust protein pore sensors on-chip has spurred development of devices incorporating artificial nanochannels. 87-nm colloid particles have been detected with a quartz nanochannel,[8] and λ-phage DNA[60] and 510-nm streptavidin-modified particles[61] have been detected with a similar PDMS device (Figure 5D). The latter device was used for both inhibition and sandwich immunoassays; diameter changes as small as 1.6 nm were detected.

Related detection methods relying on changes in nanochannel conductance have also been developed. Using a nanogap detector inside a nanofluidic channel, a 1.1-kbp DNA strand was linearized and detected as it passed between two 45-nm wide, 18-nm thick metal nanowire electrodes.[62] Linearization of the DNA inside the nanochannel minimized noise from random motion of the molecule outside the sensing element. Another detection method is based on the change in conductance caused by multiple analyte molecules binding to nanochannel walls. Streptavidin binding to a biotinylated nanochannel surface was detectable using either passive[7] or electrokinetic[63] analyte transport. Because streptavidin is negatively charged, binding increased nanochannel conductance. In general for these techniques, the output signal depends on both analyte size and charge. Additionally, sophisticated current-based sensing applications have been demonstrated using single nanopores bathed in bulk solution,[64] and multiple pores can be used simultaneously to increase sensitivity without significantly increasing signal complexity.[65] Integration of these sensors with microchannel architectures could eventually allow label-free single-molecule detection to be combined with precise fluid handling and highly efficient separations on microfluidic devices.

OUTLOOK

The properties of nanofluidic channels translate into unique technologies for integrated micro- and nanofluidic devices. Nanoscale elements can be applied to a variety of analytical tasks, from sample preparation to detection. The appropriate choice of nanofluidic components depends on the sample volume and properties, including analyte size, charge, and hydrophobicity, as well as the information to be obtained. At present, most laboratories developing applications for nanofluidic devices also specialize in fundamental studies of nanoconduits. This is unsurprising because many phenomena related to nanofluidics are not yet completely understood, and successful application of nanofluidic devices requires careful consideration of multiple interconnected variables, including device dimensions, double-layer thickness, ionic strength, and surface properties.

We expect that this technology—like microfluidics before it—will soon be accessible to non-specialists. Polymer nanopore membranes, which can be purchased with the nanofluidic elements pre-fabricated, are a likely starting point. As a deeper understanding of relevant phenomena is obtained, new and more sophisticated applications for nanochannels in lab-on-a-chip systems will be possible, but the field is presently an exciting mix of fundamental investigations and preliminary applications.

ACKNOWLEDGMENT

This work was supported in part by NSF CHE-0750295, NSF CHE-0832651, and a Merck Research Laboratories fellowship for M.L.K.

Stephen C. Jacobson is an associate professor of chemistry at Indiana University where his group and he are developing microfabricated instrumentation and using this instrumentation to study various chemical and biochemical problems. Presently, their primary areas of research are microfluidic separations, nanofluidic transport and sensing, photolithographic mapping, cell-based assays, and programmable microfluidics. Michelle L. Kovarik is currently a graduate student in Professor Jacobson's laboratory. Her research interests include nanofabrication and application of nanofluidic devices to small-volume fluid handling, particle trapping, resistive-pulse sensing, selective ion transport, and bacterial chemotaxis. Address correspondence to Jacobson at the Department of Chemistry, Indiana University, 800 E. Kirkwood Ave. Bloomington, IN 47405 (jacobson@indiana.edu).

REFERENCES

(1) West, J.; et al. *Anal. Chem.* **2008**, *80*, 4403–4419.
(2) Gates, B. D.; et al. *Chem. Rev.* **2005**, *105*, 1171–1196.
(3) Schoch, R. B.; et al. *Rev. Mod. Phys.* **2008**, *80*, 839–883.
(4) Höltzel, A.; Tallarek, U. *J. Sep. Sci.* **2007**, *30*, 1398–1419.
(5) de Jong, J.; et al. *Lab Chip* **2006**, *6*, 1125–1139.
(6) Zhou, K.; et al. *J. Am. Chem. Soc.* **2008**, *130*, 8614–8616.
(7) Karnik, R.; et al. *Nano. Lett.* **2005**, *5*, 1638–1642.
(8) Saleh, O. A.; Sohn, L. L. *Rev. Sci. Instrum.* **2001**, *72*, 4449–4451.
(9) Han, J.; Craighead, H. G. *J. Vac. Sci. Technol. A* **1999**, *17*, 2142–2147.
(10) Bayley, H.; Cremer, P. S. *Nature* **2001**, *413*, 226–230.
(11) Noblitt, S. D.; et al. *Anal. Chem.* **2007**, *79*, 6249–6254.
(12) Long, Z.; et al. *Electrophoresis* **2006**, *27*, 4927–4934.
(13) Kim, B. Y.; et al. *J. Am. Chem. Soc.* **2007**, *129*, 7620–7626.
(14) Pu, Q.; et al. *Nano. Lett.* **2004**, *4*, 1099–1103.
(15) Wang, Y.-C.; et al. *Anal. Chem.* **2005**, *77*, 4293–4299.
(16) Wang, Y.-C.; Han, J. *Lab Chip* **2008**, *8*, 392–394.
(17) Kovarik, M. L.; Jacobson, S. C. *Anal. Chem.* **2008**, *80*, 657–664.
(18) Kovarik, M. L.; Jacobson, S. C. *Anal. Chem.* **2007**, *79*, 1655–1660.
(19) Huh, D.; et al. *Nat. Mater.* **2007**, *6*, 424–428.
(20) Kuo, T.-C.; et al. *Anal. Chem.* **2003**, *75*, 1861–1867.
(21) Kalman, E. B.; et al. *Adv. Mater.* **2008**, *20*, 293–297.
(22) Oh, Y.-J.; et al. *Lab Chip* **2008**, *8*, 251–258.
(23) Karnik, R.; et al. *Nano. Lett.* **2005**, *5*, 943–948.
(24) Karnik, R.; et al. *Appl. Phys. Lett.* **2006**, *88*, 123114.
(25) Harrell, C. C.; et al. *J. Am. Chem. Soc.* **2004**, *126*, 15,646–15,647.
(26) Schmuhl, R.; et al. *Angew. Chem., Int. Ed.* **2006**, *45*, 3341–3345.
(27) Huang, J. L.; et al. *Macromolecules* **2006**, *39*, 5546–5554.
(28) Alarie, J. P.; et al. In *Micro Total Analysis Systems 2001*, Proceedings of the 5th International Conference on Micro Total Analysis Systems, Monterey, CA, Oct 21−25, 2001; Ramsey, J. M. and van den Berg, A., Eds.; Kluwer Academic Publishers: Dordrecht, The Netherlands, 2001; 131−132.
(29) Ismagilov, R. F.; et al. *Anal. Chem.* **2001**, *73*, 5207–5213.
(30) Fa, K.; et al. *J. Am. Chem. Soc.* **2005**, *127*, 13,928–13,933.
(31) Jeon, S.; et al. *Nano. Lett.* **2005**, *5*, 1351–1356.

(32) Chang, I.-H.; et al. *Environ. Sci. Technol.* **2005**, *39*, 3756–3761.
(33) Iannacone, J. M.; et al. *Electrophoresis* **2005**, *26*, 4684–4690.
(34) Eijkel, J. C. T.; van den Berg, A. *Electrophoresis* **2006**, *27*, 677–685.
(35) He, B.; et al. *Anal. Chem.* **1998**, *70*, 3790–3797.
(36) Cabodi, M.; et al. *Anal. Chem.* **2002**, *74*, 5169–5174.
(37) Kaji, N.; et al. *Anal. Chem.* **2004**, *76*, 15–22.
(38) Viovy, J.-L. *Rev. Mod. Phys.* **2000**, *72*, 813–872.
(39) Han, J.; Craighead, H. G. *Science* **2000**, *288*, 1026–1029.
(40) Fu, J.; et al. *Appl. Phys. Lett.* **2005**, *87*, 263902.
(41) Fu, J.; et al. *Nat. Nanotechnol.* **2007**, *2*, 121–128.
(42) Vankrunkelsven, S.; et al. *J. Chrom. A* **2006**, *1102*, 96–103.
(43) Rice, C. L.; Whitehead, R. *J. Phys. Chem.* **1965**, *69*, 4017–4024.
(44) Ramsey, J. M.; et al. In *Micro Total Analysis Systems 2002*, Proceedings of the 6th International Conference on Micro Total Analysis Systems, Nara, Japan, Nov 3−7, 2002; Baba, Y., Eds.; Kluwer Academic Publishers: Dordrecht, The Netherlands, 2002; Vol. 1, 314−316.
(45) Pennathur, S.; et al. *Anal. Chem.* **2007**, *79*, 8316–8322.
(46) Garcia, A. L.; et al. *Lab Chip* **2005**, *5*, 1271–1276.
(47) Pennathur, S.; Santiago, J. G. *Anal. Chem.* **2005**, *77*, 6782–6789.
(48) Wolfrum, B.; et al. *Anal. Chem.* **2008**, *80*, 972–977.
(49) Stavis, S. M.; et al. *Lab Chip* **2005**, *5*, 337–343.
(50) Foquet, M.; et al. *Anal. Chem.* **2004**, *76*, 1618–1626.
(51) Chansin, G. A. T.; et al. *Nano. Lett.* **2007**, *7*, 2901–2906.
(52) Foquet, M.; et al. *Anal. Chem.* **2002**, *74*, 1415–1422.
(53) Riehn, R.; et al. *Proc. Natl. Acad. Sci.* **2005**, *102*, 10,012–10,016.
(54) Stavis, S. M.; et al. *J. Appl. Phys.* **2005**, *98*, 044903.
(55) Heins, E. A.; et al. *Nano. Lett.* **2005**, *5*, 1824–1829.
(56) Mukhopadhyay, R. *Anal. Chem.* **2009**, *81*, 1736–1740.
(57) Suzuki, H.; et al. *Langmuir* **2006**, *22*, 1937–1942.
(58) Malmstadt, N.; et al. *Nano. Lett.* **2006**, *6*, 1961–1965.
(59) Hromada, L. P.; et al. *Lab Chip* **2008**, *8*, 602–608.
(60) Saleh, O. A.; Sohn, L. L. *Nano. Lett.* **2003**, *3*, 37–38.
(61) Saleh, O. A.; Sohn, L. L. *Proc. Natl. Acad. Sci.* **2003**, *100*, 820–824.
(62) Liang, X.; Chou, S. Y. *Nano. Lett.* **2008**, *8*, 1472–1476.
(63) Schoch, R. B.; et al. *Nano. Lett.* **2007**, *7*, 3895–3900.
(64) Gyurcsanyi, R. E. *TrAC* **2008**, *27*, 627–639.
(65) Ervin, E. N.; et al. *Anal. Chem.* **2009**, *81*, 533–537.

AC900614K